Metabolic plasticity drives mechanisms of PARP inhibitor persistence in ovarian cancer

ONE SENTENCE SUMMARY:

Ovarian cancer cells exploit metabolic plasticity to switch their glutamine/glucose metabolism to persist PARP inhibitor treatment.

AUTHORS

Adriana Del Pino Herrera[1,a] (adelpinoherrera@ufl.edu)
Joon-Hyun Song[2,3,a] (joon-hyun.song@stonybrook.edu)
Karla Torres-Arciga[2,4], (karla.torres-arciga@stonybrook.edu)
Susoma Halder[2], (susoma.halder@stonybrook.edu)
Kadin El Bakkouri[1], (kelbakkouri@ufl.edu)
Mehdi Damaghi, PhD[2,3,6,b*] (mehdi.damaghi@stonybrookmedicine.edu)
Meghan C. Ferrall-Fairbanks, PhD[1,7,b,*] (mferrall.fairbanks@bme.ufl.edu; ORCID: 0000-0002-3380-6989)

AFFILIATIONS

[1] J. Crayton Pruitt Family Department of Biomedical Engineering, University of Florida, Gainesville, FL 32611, USA
[2] Stony Brook Cancer Center, Stony Brook Medicine, Stony Brook University, Stony Brook, NY, USA
[3] Department of Applied Mathematics and Statistics, Stony Brook University, Stony Brook, NY, USA
[4] University of Mexico
[5] Department of Undergraduate Biology, Stony Brook University, Stony Brook, NY, USA
[6] Department of Pathology, Stony Brook Medicine, Stony Brook University, Stony Brook, NY, USA
[7] University of Florida Health Cancer Center, University of Florida, Gainesville, FL 32611, USA
[a,b] authors contributed equally

CORRESPONDENCE

[*] To whom correspondence should be addressed.
Correspondence on experimental section:
Mehdi Damaghi, PhD: mehdi.damaghi@stonybrookmedicine.edu
Correspondence on computational analysis:
Meghan C. Ferrall-Fairbanks, PhD
Assistant Professor, University of Florida, J. Crayton Pruitt Family Department of Biomedical Engineering
P.O. Box 116131, Gainesville, Florida 32611; O: 352-846-2762, Email: mferrall.fairbanks@bme.ufl.edu

COMPETING INTERESTS

The authors declare that there are no conflicts of interest.

ABSTRACT

Ovarian cancer results in the death of 1 in 6 patients within the first three months of diagnosis, making it the fifth deadliest cancer in the United States. While clinicians have moved towards using targeted therapies, patients often stop responding to the treatment. In this study, we combined both experimental and computational techniques to explore this process by treating OVCAR3 cell line with Olaparib (a PARP inhibitor). We then performed single cell RNA sequencing on both naïve and persistent populations. RNA velocities analysis indicated that there was a trajectory of gene expressions adaptation toward the persister phenotype. To further investigate the persistence mechanism, metabolic pathways were scored on our single cell data, and persistence cells were found to have differentially expressed glutamine metabolism compared to naïve cells. To test these findings, both persistent and naïve cells where cultured in glutamine deprived media and we found persistent cells have higher viability than the naïve cells particularly under Olaparib treatment. We then found that these cells acquired glucose dependency that can be used as vulnerability. This finding suggested increased plasticity of cancer cells under long-term Olaparib treatment. We then built a math model that suggested treatment scheduling could be improved by considering metabolic plasticity in response to Olaparib treatment.

KEYWORDS: Ovarian cancer, PARP inhibitor resistance, metabolic plasticity, glutamine and glucose metabolism

INTRODUCTION

Ovarian cancer is the fifth deadliest cancer in the United States, accounting for 19,710 patients diagnosed and 13,270 deaths from the disease in 2023 [1]. Ovarian tumors can spread to close by and remote organs with the most common metastatic sites including the uterus, ovaries, and fallopian tubes [2]. The difficulty in ovarian cancer diagnosis is due to its unremarkable symptoms, where 70% of cases are diagnosed at advanced stages when the cancer has already metastasized [3]. This has led to the death of 1 in 6 patients within the first three months of diagnosis and a 5-year survival rate of 50.8% [1]. Current treatment strategies involve the surgical removal of the tumor, if the cancer is localized, followed by adjuvant chemotherapies. These therapies are often platinum and taxane-based agents, which are assumed to be effective at the onsets of the disease. If the cancer has metastasized, neoadjuvant chemotherapies will be administered before surgical resection. These chemotherapeutic agents are delivered systemically, which leads to severe toxicities in the patients. In hopes to decrease toxicity, clinicians recently shifted towards the use of targeted therapies either before or after chemotherapy treatment.

Poly ADP-ribose polymerase (PARP) inhibitors are one of the most successful targeted therapies used against ovarian cancer [4]. The PARP enzyme is involved with fixing single-strand DNA (ssDNA) damage. PARP inhibitors (PARPis) bind to PARP, making PARP unable to repair ssDNA damages leading to double-strand breakages in the DNA, ultimately resulting in cell death. PARP is not the only enzyme able to repair DNA damages in cells [5]. A process called homologous recombination led by BRCA1/2 can repair double-strand damages to ensure cell viability. However, many ovarian cancer patients often have BRCA mutations and use PARP as a repair system, making PARPi a great therapeutic option [6]. The effectiveness of PARPis therapy has been shown in clinical trials, where the risk of recurrence on BRCA-deficient ovarian cancer patients was reduced by 40-70%, and half of the patients experienced a 5-year progression-free survival [7].

Independent of BRCA status, not all patients respond positively to PARPis and most eventually acquire resistance to the treatment [4]. More than 40% of patients with BRCA1/2 mutations do not respond to PARPis, and several patients will develop resistance after prolonged administration to these therapies [8]. Similar to other cancers, ovarian cancer cells eventually evolve resistance to targeted therapy and thus combination therapies should be considered [9], [10]. Therefore, here we aim to identify mechanisms of PARPis resistance using single cell transcriptomics and population dynamics modeling. Temporary resistance, or persistence, was developed in OVACR3 ovarian cancer cell line by treating cells for two months at low doses of a commonly used PARPi, Olaparib. Both naïve and persistent OVCAR3 cells' whole transcriptomes were studied using droplet based single-cell RNA sequencing technique. Based on scoring of major metabolic pathways [11], [12] and RNA velocity analyses [13]–[15], we

showed metabolic plasticity is evolved as mechanism of resistance that could be used as vulnerabilities. These indicated that the development of persistence in ovarian cancer can be tied to regulation of glutamine metabolism. We then validated this finding by combining the Olaparib treatment and glutamine deprived media showing OVCAR3 persister cells indeed have higher viability and growth than naïve cells in glutamine deprived media. Then we performed Seahorse experiments and discovered a higher glycolytic capacity in persister cells evolved under Olaparib treatment that justifies the energy needs of persister cells. In this paper, we have integrated experimental and mathematical techniques to provide a better understanding of PARPis effects on ovarian cancer at the cellular level, indicating metabolic plasticity in persistent populations. We proposed to add metabolic switching in PARPi adaptive therapy design to target metabolic plasticity as a vulnerability for at least a subpopulation of ovarian cancer cells.

RESULTS

Olaparib persistence phenotype described at single-cell resolution in OVCAR3

To study the mechanisms of PARPis persistence in ovarian cancer, we performed single-cell RNA sequencing (scRNAseq) on OVCAR3 ovarian cancer cell line naïve to Olaparib and treated for two months. We used the term persistence over resistance because we could never reach to a full resistance phenotype meaning that even after 6 month under PARPi, as soon as we remove the drug from the media the cells went back to their parental drug sensitive phenotype [16]. PARP inhibitor persistence was developed by treating OVCAR3 with Olaparib at 10 μM for two months (**Fig. 1A**). After persistent lines were developed, cell viability for the parental (naïve) and persistent cell populations were assessed using Cell Counting Kit-8 (CCK-8) viability assay (n=3) at different treatment concentrations (0, 5, 10, 25, 50, 100 μM Olaparib). Naïve cells showed higher sensitivity to PARPi at drug concentration of 10uM. At 25, 50, and 100 μM Olaparib treatment conditions, persistent cells had higher viability implying the development of the drug tolerance (**Fig. 1B**). This observation is in line with recent studies showing increased adaptability of cancer cells to PARPi [17].

Parental and persistent cells were then sequenced at a single-cell resolution using the 10X Genomics Chromium technology to identify the different transcriptomic states between naïve and persistent populations. A total of 2,348 cells were sequenced (1,766 naïve and 582 persistent) and filtered to remove low-quality cells. The cell number after filtering was reduced to 2,262 (96%), which were then log-normalized, scaled, and dimension reduction was performed using principal component analysis. Graph-based clustering was used to identify phenotypically defined clusters and visualized using UMAP. Based on cell identify, the naïve and persistent populations have two distinct areas that can be characterized by five distinct phenotypic clusters (**Fig. 1C-D**). All the clusters identified contained mixed populations of both naïve and persistent cells, suggesting that the development of persistence might be closely related to the initial naïve phenotype. However, clusters 0, 3 and 4 express a higher proportion of naïve

cells (98%, 99%, and 98%, respectively) whereas cluster 1 is 98% composed of persistent cells.

Metabolic signature analysis of OVCAR3 naïve and persistent populations indicate glutamine dependency

To understand the transcriptomic dynamics taken place in the adaptation of naïve towards persistent phenotype transition, RNA velocities were calculated for the entire dataset. RNA velocities indicated the speed at which unprocessed, or raw, RNA compared to processed RNA and how that changes overtime [14]. These changes are indicators of gene expression upregulation, which inform what genes or cluster within the dataset were associated with the transition between naïve and persistent states. Initially, RNA velocities were calculated as a deviation from the steady-state of gene expression across all cells. An algorithm, called scVelo, improved upon this steady-state assumption by creating four transcriptional states, initially following the four states of endocrine cell formation in a dynamical model [13], [14]. For the OVCAR3 dataset, a velocity graph was initially obtained using scVelo with the top 2000 highly variable genes with at least 20 mRNA reads and normalizing the counts for each cell (**Fig. 2A**). The velocity vectors indicated that cells in most clusters have the potential to transition to a transcriptomic state similar to cells in cluster 1 (Clus1). Clus1 (indicated in orange in **Fig. 2**) had the highest proportion of persistent cells, which suggests that a transcriptomic mechanism could be responsible for this transition. The latent time of different clusters was also computed confirming that progression of the dynamics process ends with Clus1 (**Fig. 2B**). That velocity graph was then utilized as part of the data preprocessing to then run DeepVelo [15]. DeepVelo computed specific kinetics for each cell instead of assuming that each gene will travel in the same velocity trajectory. DeepVelo added noise to the dataset to train a variational autoencoder into an ordinary differential equation model, which captured changes in gene expression within a cell over time. The velocity graphs obtained using DeepVelo showed similar results as those obtained with scVelo (**Fig. 2C**). Once again, the RNA velocities move towards Clus1, suggesting a transcriptomic transition from other clusters towards Clus1.

RNA velocity indicated a transcriptomic transition between clusters with a high proportion of naïve cells (clusters 0, 3, and 4) and Clus1, which contained a high proportion of persistent cells. We focused on pathways tied to differentially expressed genes within each population (naïve and persistent) that could drive the transition between phenotypes. Differentially expressed genes were identified as those detected at a minimum fraction of 0.25 and at 0.25-fold difference between all the cells in the dataset. Differentially expressed genes in clusters 0, 3 and 4, which were primarily composed of naïve cells, and in cluster 1, which was primarily composed of persistent cells, were then input into Enrichr [18] and the Reactome pathways annotations were collected (**Fig. 2D**, **Supplemental Table T1**). For both naïve and persistent clusters, pathways related to cell cycle were differentially expressed. This aligns with the mechanism of action of PARPi treatment which directly affects the cell cycle. Both groups presented high expression of cell cycle checkpoints, where naïve clusters highly expressed genes related to S phase and the persistent cluster highly expressed genes

related to the G2/M transition. This trend is supported by other works related to the mode of action of PARPi drugs [19], [20].

Another main difference in pathway expression between the populations was in the glutamate and glutamine metabolism. This pathway was differentially expressed between naïve and persistent population, which suggests persistent cells may have regulated their glutamine metabolism. We then evaluated the expression of 1,456 genes linked to 42 KEGG [21] metabolic pathways including glutamine metabolism, to test the hypothesis that persistence may be related to glutamine dependence. A score was calculated for each cell based on the expression of the gene list associated with each pathway. The glutamine metabolism scores showed a difference of $p<0.0001$ between the naïve and persistent populations (**Fig. 2E**). Additionally, when the gene list for glutamine metabolism was interrogated within the latent time in DeepVelo, glutamine metabolism genes (PYCR3, RMLKLB, and GLS) were part of the highly variables genes (**Fig. 2F**). These glutamine metabolism genes appear towards the tail end of the latent time; of particular note is the GLS gene, which encodes for the glutaminase protein responsible for the first reaction in the glutamine metabolism. These results suggest that there is a significant regulation of glutamine metabolism in persistent cells.

OVCAR3 persistent cells increased glycolytic capacity and metabolic plasticity to Olaparib treatment

To further investigate glutamine metabolism regulation in response to PARPi treatment, both naïve and persister cells were cultured in media with 0 μM Olaparib (untreated) with and without glutamine (Gln+ and Gln- respectively) and 50 μM Olaparib (treated) with and without glutamine (Gln+ and Gln- respectively). CCK-8 assay was performed to determine the effects of glutamine deprivation with and without Olaparib treatment on cell viability after one week of treatment (n=3). The viability of the naive cells decreased by 35% when they are treated with Olaparib and Gln+, while the viability of the persistent population remained 100% under those conditions (**Fig. 3 A and B**). When glutamine was depleted from the media in absence of Olaparib, the viability dropped dramatically by 72% and 48% for both naive and persistent populations, respectively compared to 0 μM Olaparib/Gln+ media. Signifying that depleting the cells from glutamine affects viability of naïve cells more greatly than persister cells implying their less dependency to glutamine. However, under Olaparib treatment in glutamine-deprived media, the viability of naïve cells slightly dropped by 8%, while that of the persistent populations stayed the same, suggesting under PARPi treatment both naïve and persister cells are less dependent of glutamine metabolism. This fast metabolic switch in both cells confirm the cancer cells metabolic plasticity. Also, higher viability in the persistent population suggests that cells could be upregulating their intrinsic glutamine production to withstand the effects of the drug and the lack of glutamine in the environment. These results led us to hypothesize that, upon PARPi treatment, cancer cells prioritize glutamine for DNA repair over energy production. To test whether cancer cells shift their metabolism toward glycolysis, we

performed a Seahorse analysis to measure cells glycolytic phenotype comparing to their mitochondrial respiration under Olaparib treatment with and without glutamine. We found that both naïve and persister cells treated with Olaparib in the presence of glutamine have increased extracellular acidification rate (ECAR) implying the increased glycolysis and switching to glucose metabolism. Interestingly, glutamine deprivation decreases both naïve and persister cells mitochondrial respiration and glycolysis dramatically. However, when treated with Olaparib the glycolysis is increased to basal level. This metabolic plasticity persisted in persister cells, which maintained higher glycolysis levels even in the absence of treatment (**Fig. 3C and 3D**). Analysis of the oxygen consumption rate (OCR) indicates a decrease upon treatment with PARP inhibitors in both naïve and persistent cells, corroborating the ECAR data and suggesting a metabolic shift towards increased glycolysis (**Fig. 3E**).

Mathematical modelling simulations of naïve and persistent cells show a decrease in cumulative drug dosages for glutamine deprivation and adaptive therapy schedules compared to continuous therapy schedules

Mechanistic mathematical modelling was used to study cell growth dynamics over time under different environmental conditions (0μM Olaparib, 20μM Olaparib, Gln+, and Gln- conditions). Cell counts were collected every 48-72 hours for 772 hours (n=5-18) (**Supplemental Figure S1**) and were cultured in well plates, which constrain exponential growth in a density-dependence manner. Therefore, a logistic growth model was selected to model the growth dynamics of these populations *in vitro*. Logistic growth assumes a dependence of population growth rate on population density [3]. When the total population reaches a carrying capacity then it will stop growing. Logistic growth is described as:

$$\frac{dN}{dt} = rN(1 - \frac{N}{K})$$

where *N(t)* is the population size at time *t*, *r* is the cell growth rate (in hours^{-1}), and *K* is the carrying capacity. Cell counts were normalized by the counts on day 0 to have a better representation of population dynamics across all conditions. These counts were used to estimate logistic growth rates (r) and carrying capacities (K) in Julia by minimizing the sum of squared errors between experimental data and the model. Estimated logistic growth curves for each cell population (OVCAR3 naïve and persistent) were computed under 0μM Olaparib/Gln+ environmental conditions (**Supplemental Table T2**). In terms of growth rates, persistent cells present a higher growth rate than naïve cells. However, naïve cells have a higher carrying capacity than persistent cells indicating that under standard media conditions (0μM Olaparib/Gln+) naïve cell will dominate in the population.

The growth rates and carrying capacities estimated for naïve and persistent cells under untreated and glutamine added conditions were used to create co-culture simulations between these populations across the different media conditions and

different initial persistence percentage. This co-culture model was described using the following equations:

$$\frac{dN}{dt} = r_N\left(1 - \frac{N+P}{K_N}\right) - \alpha_N PARP * N - \beta_N(1 - GLN) * N$$

$$\frac{dP}{dt} = r_P\left(1 - \frac{P+N}{K_P}\right) - \alpha_P PARP * P - \beta_P(1 - GLN) * P$$

$$T(t) = N(t) + P(t)$$

where *N(t)* and *P(t)* are the naïve and persistent population sizes at time *t*, r_N and r_p are the cell growth rate (in hours^{-1}), and K_N and K_P are the carrying capacities for the naïve and persistent population previously estimated under untreated and glutamine added conditions. The effect of treatment and glutamine deprivation was modelled as an on and off term that would change based on the magnitude of the factors of α_N and α_P for treatment effect and β_N and β_P for glutamine deprivation. These terms were estimated for naïve and persistent populations individually by fitting the above equations, which contained the growth rates and carrying capacities under untreated and glutamine added conditions, to the data collected using different media conditions. For instance, different α_N and α_P were calculated for glutamine added and glutamine deprived media conditions. Similarly, different β_N and β_P were calculated for both untreated and treated conditions. Generally, $\alpha_N > \alpha_P$ both under glutamine added and glutamine deprived media which is consistent with previous results of Olaparib greatly affecting the viability of naïve cells while maintaining viability of the persistent group. Additionally, $\beta_N > \beta_P$ both under untreated and treated conditions indicating that glutamine deprivation affects the naïve population more. This is reflected in the co-culture simulations (**Figure 4**). Co-culture simulations under four different continuous media conditions (0μM Olaparib/Gln+, 0μM Olaparib/Gln-, 20μM Olaparib/Gln+, and 20μM Olaparib/Gln-) and three different initial persistence percentages (25%, 50%, and 75%) were initially created across 768 hours. Under these four continuous media conditions and 25% initial persistence, naïve cells initially dominate in the population. However, naïve cells are only dominant by 768 under standard media conditions (0μM Olaparib/Gln+) and 25% initial persistence. Focusing on the total population growth, glutamine deprivation under untreated conditions (0μM Olaparib/Gln-) causes a 0.64-fold decrease in the total population by 768 hours across all initial persistence percentages compared to standard conditions (0μM Olaparib/Gln+). Olaparib treatment alone (20μM Olaparib/Gln+) only causes a 0.13-fold decrease in the total population compared to standard conditions. However, when both glutamine deprivation and treatment are combined (20μM Olaparib/Gln-) then the total population experiences a decrease of 0.85-fold compared to standard conditions. This indicated that the combination of glutamine deprivation and Olaparib treatment at the tumor site can achieve a greater cancer population size reduction than treatment alone. In order to achieve this decrease in the total population, a cumulative drug dose of 340μM Olaparib (20μM delivered every 48 hours) is necessary. This cumulative dosage will result in several patient toxicities and complications in treatment.

To minimize cumulative drug dosages, in the addition to the four continuous media conditions already simulated, two different adaptive treatment schedules were also tested similar to Strobl et al. schedules [16]. For both schedules, the glutamine was either present or deprived (Gln+ or Gln- respectively). The first schedule (AT modulating) consisted in dynamically adjusting the drug dosage based on changed in the total population size. If the population changed by 10% in 48 hours, then the drug dosage would be adjusted by 5μM. For example, if the total population size decreased by 10% then the drug dosage would decrease by 5μM (until it reached 0μM). If the population later increased by 10% then the drug dosage would increase by 5μM, reaching a maximum drug concentration of 20μM. The second schedule (AT skipping) consisted of skipping treatment periods if there was a total population reduction of 10% in a 48-hour period. Both schedules began by treating the population at an Olaparib concentration of 20μM and either modulating or skipping a dose (setting the treatment to 0μM) when the population decreased by 10%. For both schedules, glutamine deprived conditions (Gln-) showed a reduction in cumulative drug dosages. The lowest cumulative drug dosage was achieved through the glutamine deprived adaptive therapy skipping schedule (180μM cumulative dose). Compared to the continuous glutamine deprived and treated conditions (20μM Olaparib/Gln-), AT Skipping/Gln- results in a 0.63-fold increase in the total population by 768 hours while nearly utilizing nearly half the amount of Olaparib. Therefore, adaptive therapy is able to achieve similar results to continuous treatment in terms of total population size but using much lower values of drug. Glutamine deprivation and adaptive treatment has the potential to reduce treatment toxicities while achieving tumor control.

DISCUSSION

Ovarian cancer is the second most lethal gynecological disease characterized by high tumor heterogeneity. The nature of the disease increases treatment challenges resulting in a high probability of recurrence even to targeted therapies such as PARPi. Our study aimed to explore the mechanisms of persistence development at the transcriptomic and cellular dynamics levels of an established high-grade serous ovarian cancer cell line, OVCAR3. Initially, persistence was developed over two months with Olaparib treatment, which was confirmed with CCK-8 assay and both parental (naïve) and persistence populations were sequenced using droplet-based scRNAseq. As opposed to bulk sequencing, scRNAseq allowed us to study phenotypic and molecular differences at an individual cell level, capturing a higher resolution picture of cellular heterogeneity including potentially rare populations.

Graph-based clustering identified 5 distinct clusters, all composed of both naïve and persistent cells at different proportions. However, the predominately naïve or persistent cell composition of some clusters was useful to identify a potential transcriptomic transition between the phenotypes. This transition was studied through the directionalities of RNA velocity vectors developed using scVelo and DeepVelo. The distribution of the clusters throughout the latent time showed Clus1, which contains the highest proportion of persistent cells, at the end of this progression, which suggested a transcriptomics switch between the two populations. To understand the difference

between the populations, the differentially expressed genes were obtained to determine the top significantly expressed Reactome pathways. The main difference between naïve and persistent differentially expressed pathways was the upregulation of the glutamine metabolism in the persistent population. Glutamine plays a crucial role in the body by maintaining and promoting cell functions such as protein synthesis and serving as a precursor for nucleotide and neurotransmitter synthesis [22]. Further metabolic pathway scoring analysis using genes from 42 different metabolic pathways showed a significant difference between naïve and persistent populations scores for the glutamine metabolism. One of the main gene players for this metabolism is the GLS gene. GLS encodes for an enzyme called glutaminase whose role is to convert glutamine to glutamate so it can be utilized in multiple pathways such as the tricarboxylic acid (TCA) cycle or amino acid synthesis [23]. In our RNA velocity analysis, we were able to show that the GLS gene is expressed at the end of the latent time. Clus1, which is predominantly composed of persistent cells is the last cluster on the latent time, indicating that the expression of GLS is characteristic of persistent cells. Thus, the glutamine metabolism could be the one responsible for OVCAR3 persistence to Olaparib.

Our findings support that PARPi drugs act while the DNA is replicated during S phase, resulting in naïve cells arresting in S phase. Persistence cells can evade the effects of PARPi (**Fig. 2D**) and these cells suggest are highly expressed in the G2/M transition pathway, which can allow them to continue proliferating [24]. In addition, persistent cells express p53-dependent G1 DNA damage response, which allows damaged cells to arrest in G1 phase, while their DNA is being repaired before moving to replication or S phase [25]. Once again, this pathway offers a mechanism around the effects of PARPi through DNA reparation. While persistent cells highly express pathways contributing to cellular growth, naïve cells highly express immune response pathways such as the signaling by Rho GTPases. These proteins are crucial for the initiation and progression of tumors, as well as interactions with the tumor microenvironment and the regulation of inflammatory responses [26].

One-week cell viability experiments under different media conditions combining the presence and absence of Olaparib and glutamine, showed that the viability of persistent cells is not affected under treated and glutamine deprived media compared to the untreated and glutamine deprived media. Whereas the viability of naïve cells decreased when treatment was added to glutamine deprived media. Growth curves of naïve and persistent cells created by estimating growth parameters through mathematical modeling under different media conditions showed a similar trend. While a lower growth rate was estimated for naïve cell compared to persistent cells, these cells presented a higher carrying capacity indicating naïve cell dominance in the population when combined with persistent cells. When evaluating the effects of treatment and glutamine deprivation in these populations, parameter estimation showed that the growth of naïve cells is more negatively affect under treated or glutamine deprived conditions compared to persistent cells. This suggests that persistent populations are intrinsically upregulating their glutamine metabolism to be able to sustain the lack of this protein in their environment. When evaluating co-culture simulations of naïve and persistent populations, it was observed that both the effects of treatment and the effects of glutamine deprivation affect the growth of the naïve population more negatively

compared to persistent. However, these simulations show the potential effectiveness of the combination of Olaparib and glutamine deprivation. While total population decrease is observed in both continuous and adaptive therapy schedules, adaptive therapy is able to achieve a much lower cumulative drug dosage. In this scenario, adaptive therapy has the potential of achieving the control of the total population as well as the ability to greatly decrease the cumulative drug dosage across the treatment schedule. Moreover, adaptive therapy combined with glutamine deprivation has the potential to not only provide tumor control but to decrease treatment toxicities in patients since cumulative drug dosages would be much lower than continuous treatment schedules.

Previous research has shown that glutamine depletion has avoided the development of resistance to chemotherapeutics in cancers such as pancreatic or liver cancer [27]. In these cancer cell populations, cells upregulated their glutathione synthesis, the successor to the glutamine metabolism, to protect themselves from the effects of chemotherapy. In cancers such as breast, sarcoma and ovarian there is an upregulation of the glutathione metabolism as well when treated with different chemotherapies [28]. However, we did not see the same trend in our study of cells treated with PARP inhibitors. The hypothesis that PARPi treatment causes cancer cells to shift glutamine metabolism toward DNA repair rather than energy production highlights an intriguing adaptive mechanism in cancer cell survival. PARP inhibitors, like Olaparib, target DNA damage repair pathways by inhibiting the PARP enzyme, which is crucial for repairing single-strand breaks in DNA. This puts significant stress on the cancer cells' ability to manage DNA damage. In response, cancer cells may alter their metabolic pathways, such as reallocating resources like glutamine, a versatile amino acid that plays a role in both energy production and biosynthetic pathways. The hypothesis suggests that after PARPi treatment, glutamine's primary role may shift toward aiding DNA repair rather than fueling the tricarboxylic acid (TCA) cycle for energy generation. This reallocation likely reflects the cells' need to prioritize survival under DNA damage stress. To further explore this, the Seahorse analysis was used to measure metabolic shifts, particularly glycolysis. The data showed that OVCAR3 cells treated with Olaparib increased their glycolytic activity, indicating a metabolic reprogramming toward glycolysis. This quick switch is a perfect example of metabolic plasticity in cancer cells. Glycolysis offers a quicker but less efficient form of energy production compared to oxidative phosphorylation, which is typical in highly proliferative cancer cells. This shift could be a survival adaptation, allowing cancer cells to rapidly generate energy and biosynthetic intermediates under therapeutic stress. Interestingly, this metabolic phenotype appears to become fixed in persister cells—those that survive initial treatment and may lead to eventual recurrence. These cells show higher glycolytic activity even in the absence of ongoing PARPi treatment, suggesting that glycolysis has become an entrenched survival mechanism. This shift could make persister cells more resilient to further stress, such as additional rounds of chemotherapy or targeted therapies. These findings raise important considerations for combination therapies. Targeting glycolysis in conjunction with PARP inhibition might increase the therapeutic efficacy by preventing persister cell survival, which is often a major hurdle in durable cancer treatment outcomes. The role of metabolic plasticity in therapy resistance also becomes a key area of interest for future research aimed at overcoming cancer recurrence.

Our work suggests that the regulation of the glutamine metabolism could be driving persistence development in our *in vitro* model of ovarian cancer. The combination of data science, experimental, and mathematical modeling techniques have allowed to study the development of PARPi persistence in OVCAR3 through different angles which have pointed towards PARPi persistence mechanisms related to glutamine metabolism. The next steps in this line of work are to show an increased production of glutathione or glutamate in persistent cells compared to naïve as well as understanding the degree of glutamine depletion needed to avoid persistence development.

METHODS

Cell culture

OVCAR3 cells were acquired from American Type Culture Collection (ATCC) and cultured in RPMI medium (ThermoFisher) supplemented with 10% Fetal Bovine Serum and 1% penicillin/streptomycin. At all times cells were kept at 37°C and in 5% CO_2. Cells were tested for mycoplasma contamination and were authenticated before the study started.

Viability analysis (CCK-8 assay)

To measure cancer cells growth in the absence and presence of Olaparib treatment, cells were seeded in a 48 well flat-bottom plate and let them attach overnight. Media was replaced with treated growth medium, containing 0, 1, 10, 25, 50 or 100 μM Olaparib (AstraZeneca), and cell growth was monitored for 8 days. Viability assays were measured using CCK8 kit for at least 4 technical and 3 biological replicates.

Cell growth dynamics

Cell growth was monitored by imaging the cells at 4X and 10X resolution using Cytation X (Agilent) time-lapse microscopy system. Confluency was measured based on bright field images and analyzed using the Gen5 Software.

Single-cell RNA-sequencing

Chromium Single Cell 3′ Library, Gel Bead & Multiplex Kit and Chip Kit (10x Genomics) was used to encapsulate and barcode for cDNA preparation of OVCAR3 parental (naïve) and persistent cells. The libraries were constructed according to the manufacturer's protocol, sequenced on an Illumina NovaSeq and mapped to the human genome (GRCh38) using CellRanger (10x Genomics).

Raw gene expression matrices generated per sample using CellRanger (v.3.0.1) were combined in R (v.4.2.0) and converted to a Seurat object using the Seurat R package [29]. Naïve and persistent Seurat objects were merged and studied in combination for further downstream analysis. Initially, low quality cells were filtered out

of the dataset. Cells with unique feature counts under 200 and above the mean count reads plus two standard deviations were filtered from the dataset. Cells that expressed a high mitochondrial gene expression above the average expression for each cell and under 200 were also filtered. After filtering, the data was log-normalized, and the top 4287 number of highly variable features were identified using the FindVariableFeatures() function. The data was scaled to regress out variation due to differences in count and percentage of mitochondrial content. Then, a linear dimension reduction was performed using the highly variable features (PCA). A graph-based clustering approach (Louvain algorithm) was used to identify phenotypic clusters, which resulted in 5 distinct clusters composed of both naïve and persistent cells. Data was visualized using UMAP projects [30].

Differential gene expression and pathways analysis

Differentially expressed genes for the dataset were identified using the Seurat FindAllMarkers() function by selecting those detected at a minimum fraction of 0.25 and at a 0.25-fold difference across all the cells in the dataset. The gene lists detected for OVCAR3 naïve and persistent cells were input separately in Enrichr [18]. This web-based tool was able to provide differentially expressed pathways in relation to the gene list input. For both populations, the top significantly enriched pathways provided by the Reactome and Kyoto Encyclopedia of Genes and Genomes (KEGG) databases were identified. The p-values were computed using Fisher's exact test.

Metabolic pathway scoring

A list of 1,456 genes linked 37 KEGG and 5 Reactome metabolic pathways was used for gene enrichment analysis. The gene lists for each pathway was scored across each cell using the AddModuleScore() function. Scores for naïve and persistent populations were compared for each pathway using the Mann-Whitney U test.

RNA velocity analysis

Raw genome data and filtered features matrices for the naïve and persistent populations from CellRanger was input separately into Python 3 as well the clusters and UMAP embeddings assigned to each cell from the Seurat pipeline. To improve RNA velocity predictions, the information of the pre-mature (unspliced) and mature (spliced) transcripts obtained through velocyto [31] is also input into Python. Cells that were eliminated during Seurat pre-processing were also filtered out of the naïve and persistent velocyto transcript counts as well as the feature matrices. At this point the velocyto transcripts and feature matrices were merged for naïve and persistent populations to create AnnData [32] objects. For downstream analysis naïve and persistent AnnData objects were merge into an object containing 2262 total cells and

33538 features. The scVelo package [14] was used to normalize the merged dataset to a shared count of between 20 and 2000 top variable genes. The function scv.pp.moments was used to compute moments of gene expression distribution and 30 principal components and 30 nearest neighbors. The scVelo dynamical algorithm computed dynamical velocity vectors and latent times for each cell which were extracted and graphed. The deep learning algorithm DeepVelo [15], was then used to train a variational autoencoder into an ordinary differential equation model were complex genes interactions and denoised RNA velocities were obtained and graphed. Lastly, the function scv.pl.heatmap() was used to compute a heatmap of the expression the glutamine metabolism genes across the latent time.

Seahorse XF Analysis

Glycolytic rate of OVCA3 and selected OVCA3 cancer cells was measured using Seahorse XF96 extracellular flux analyzer and a MST kit (Seahorse Biosciences). OCR and ECAR of cancer cells were determined by seeding them on XF96 microplates in RPMI medium until cells reached over 90% confluence. In these studies, seeding started with 20,000 cells (80% of well area). Measurements were determined 24 h later when the cells reached the 90% confluence. One hour before the Seahorse measurements, culture media were removed, and cells were washed with PBS followed by addition of base medium (nonbuffered Dulbecco's Modified Eagle Medium supplemented with 25 mM glucose) or our nonbuffered only-glucose-containing solution. For glycolytic rate measurements, mitochondria inhibitors including rotenone (1 μM) and antimycin A (1 μM) were injected after basal measurements of ECAR and OCR of the cells under treatment to stop the mitochondrial acidification. Finally, data were normalized for cell number in each well from imaging by CytationX. Seahorse measurements were performed with four to six technical replicates, and these experiments were repeated four times.

Solutions for seahorse experiments. A total of 2 mM Hepes, 2 mM MES, 5.3 mM KCl, 5.6 mM NaPhosphate, 11 mM glucose, 133 mM NaCl, 0.4 mM MgCl2, and 0.42 mM CaCl2 were titrated to the given pH with NaOH. For reduced Cl− experiments, 133 mM NaCl was replaced with 133 NaGluconate, and MgCl2 and CaCl2 were raised to 0.74 and 1.46 mM, respectively, to account for gluconate-divalent binding. The amount of dilute HCl or NaOH added to medium to reduce pH to target level was determined empirically.

Respiratory capacity is a measure of the maximum rate of O2 consumption and mitochondrial electron transport in a cell. Glycolytic capacity is the maximum rate of glucose conversion to pyruvate and/or lactate by a cell. Glucose breakdown to two lactates produces two protons, allowing for the capability of indirect measurement of glycolytic rate using the extracellular acidification.

Mathematical modelling of OVCAR3 growth dynamics

Growth dynamics were modelled with an ordinary differential equation (ODE) logistic model described by the following expression $\frac{dN}{dt} = rN(1 - \frac{N}{K})$, where N(t) is the population size at time t, r is the cell growth rate (in day^{-1}), and K is the carrying capacity. Model parameters were estimated in Julia to estimate both r and k for the naïve and persistent populations individually under untreated and glutamine added media using the DifferentialEquations.jl [33] and DiffEqParamEstim.jl (https://www.github.com/SciML/DiffEqParamEstim.jl) packages. Cell counts were normalized by the first count read for each set of conditions to use for parameter estimation with an initial population size of 1. The ODEproblem function was used to define the problem and a loss function was created based on that ODEproblem to reduce the loss between experimental and simulated data using the Tsit5() solver and 10000 iterations. The optimized solutions returned the estimated growth rate (r) and carrying capacity (K) for the data for each population under each condition that are reported in **Supplemental Table T2**.

Co-culture model and simulations of OVCAR3 growth dynamics

Based on the recurrence development in ovarian cancer, tumors are thought to be composed of heterogenous populations of cells. In our model, we assumed naïve and persistent cells compete in the tumor microenvironment following the equations below adapted from Strobl et al. [34]:

$$\frac{dN}{dt} = r_N\left(1 - \frac{N+P}{K_N}\right) - \alpha_N PARP * N - \beta_N(1 - GLN) * N$$

$$\frac{dP}{dt} = r_P\left(1 - \frac{P+N}{K_P}\right) - \alpha_P PARP * P - \beta_P(1 - GLN) * P$$

$$T(t) = N(t) + P(t)$$

where N(t) and P(t) are the naïve and persistent population sizes at time t, r_N and r_p are the cell growth rate (in hours^{-1}), and K_N and K_P are the carrying capacities for the naïve and persistent population previously estimated under normal conditions (0µM Olaparib/Gln+). The first term of both the naïve and persistent equations represent the logistic growth rate of the populations. In this case, the competition of the populations is modelled in a Lotka-Volterra fashion where the inter- and intraspecies competition coefficients both take the value of 1.

The second and third term of the equations represent the effect of treatment and glutamine deprivation in a linear manner assuming that these terms affect cell growth

directly by a fixed amount. These terms were modelled as an on and off term that would change based on the magnitude of a factor of α_N and α_P for treatment effect and β_N and β_P for glutamine deprivation. Both the $PARP$ and GLN took values of either 0 or 1. For instance, under untreated conditions the $PARP$ term would take a value of 0 and not contribute to the growth of the population. Under treated conditions, the $PARP$ term would take a value of 1 decrease population growth by a factor of α. Contrarily, when GLN is 0 the population would experience a decrease in growth by a factor of β since this term models the effect of glutamine deprivation.

α_N and α_P for 20µM Olaparib/Gln+ were estimated individually for naïve and persistent by fitting the mono-culture data for those conditions to the ODE equations above containing the r_N, r_p, K_N and K_P previously estimated under 0µM Olaparib/Gln+. These α_N and α_P were recorded as the effect of treatment under glutamine added conditions. A similar process was followed when estimating for β_N and β_P for 0µM Olaparib/Gln-. These were also parameterized for naïve and persistent individually by fitting the mono-culture data for those conditions to the ODE equations above containing the r_N, r_p, K_N and K_P previously estimated under 0µM Olaparib/Gln+. These β_N and β_P were recorded as the effect of glutamine deprivation under untreated conditions. To estimate all α_N, α_P, β_N and β_P under 20µM Olaparib/Gln- conditions, the mono-culture data for those conditions was used to fit the ODE equations above containing the r_N, r_p, K_N and K_P previously estimated under 0µM Olaparib/Gln+. These last α_N, α_P, β_N and β_P were recorded as the effect of treatment under glutamine deprived conditions. All these parameters were estimated using the DifferentialEquations.jl [33] and DiffEqParamEstim.jl (https://www.github.com/SciML/DiffEqParamEstim.jl) packages in Julia. The ODEproblem function was used to define the problem and a loss function was created based on that ODEproblem to reduce the loss between experimental and simulated data using the Tsit5() solver and 10000 iterations. The effect of treatment and glutamine deprivation parameters are reported in **Supplemental Table T3**.

Adaptive therapy schedules simulations

Growth rates, carrying capacities, glutamine deprivation terms and treatment terms previously determined for naïve and persistent populations were used within the co-culture ODE system to create adaptive therapy schedules simulations. To implement these adaptive therapy schedules, the differential equation model was modified at specified time intervals using Julia's built-in Callback() function. This function allows for conditional triggers based on time or population state. For our simulations, treatment adjustments were made every 48 hours, with an initial drug dosage of 20 µM for all schedules. Two adaptive therapy treatment schedules were tested. The first adaptive

therapy schedule (AT modulating) dynamically adjusted the drug dosage based on the tumor population size. If the tumor grew by 10% or more, the Olaparib dosage would increase by 5μM for the next 48-hour period. Conversely, if the tumor population decreased by at least 10%, the drug dosage would be reduced by 5μM. If the tumor population showed minimal change, the drug dosage would remain unchanged for the next interval. This approach aimed to simulate a physician adjusting treatment based on tumor progression. The second adaptive therapy schedule (AT skipping) employed a dose-skipping strategy. In this schedule, if the tumor population increased by 10% or more, the dosage would be set to 20μM. If the population decreased by at least 10%, the dosage would be reduced to 0μM. If there was not a net change of at least 10% in 48 hours the drug dosage in the simulation remained the same. Thus, the drug dosage alternated between two levels: 0μM or 20μM, based on tumor size.

Both adaptive therapy schedules were tested across 768 hours and treatment values were allowed range from 20μM to 0μM, sticking to either 20μM or 0μM for the AT skipping. To evaluate the effects of glutamine, for each adaptive therapy schedule both glutamine added, and glutamine deprived conditions were evaluated.

Statistical analysis

The statistical tests were conducted in GraphPad Prism (Version 10.0.2). To analyze statistical differences between groups in CCK8 assay analysis, and between persistent and naïve populations' pathway scores we used the non-parametric Mann-Whitney U test.

DECLARATIONS

Ethics Approval and Consent to Participate: Not applicable

Consent for Publication: Not applicable

Availability of data and materials: The code and documentation describing our single-cell analysis pipeline are open-source and publicly available through the OvCa PARP Persistence GitHub repository (https://www.github.com/mcfefa/OvCa-PARP-resistance). Three virtual machines producing the full computational environment is available on Code Ocean:

- R (https://www.codeocean.com/capsule/7415977/tree),
- Python (https://codeocean.com/capsule/6361603/tree),
- Julia (https://codeocean.com/capsule/0142580/tree)

Competing Interests: The authors declare that there are no conflicts of interest.

Funding: Experimental research reported in this publication is supported by Physical Sciences Oncology Network at the National Cancer Institute through, Grant/Award Numbers: U01CA261841-01, and National Institutes of Health, Grant/Award Number: R01CA249016-01 for Dr. Damaghi's team. This work was in part supported by funding from the National Institutes of Health (NCATS KL2TROO1429, NCI R01CA278300) for Dr. Ferrall-Fairbanks' team.

Authors' Contributions:

A. Del Pino Herrera: data curation, formal analysis, investigation, software, visualization, writing-original draft, writing-review & editing.

J-H. Song, K. Torres-Acirga, S. Hadler: performed experiments and analyzed the experimental data.

K. El Bakkouri: formal analysis, software, and visualization.

M. Damaghi: MD conceived and designed the study, performed single cell experiments and analyzed the data as well as writing–original draft, writing–review and editing.

M.C. Ferrall-Fairbanks: data curation, formal analysis, investigation, methodology, project administration, resources, software, supervision, visualization, writing–original draft, writing–review & editing.

Acknowledgements: This work has been supported in part by the Molecular Genomics Facility Shared Resource at the H. Lee Moffitt Cancer Center and Research Institute, an NCI-designated Comprehensive Cancer Center (P30-CA076292). The analysis research is supported by the UF Health Cancer Center, supported in part by state appropriations provided in Fla. Stat. § 381.915 and the National Cancer Institute of the National Institutes of Health under Award Number P30-CA247796. The content is solely the responsibility of the authors and does not necessarily represent the official views of the National Institutes of Health or the State of Florida.

REFERENCES

[1] R. L. Siegel, K. D. Miller, N. S. Wagle, and A. Jemal, "Cancer statistics, 2023," *CA. Cancer J. Clin.*, vol. 73, no. 1, pp. 17–48, Jan. 2023, doi: https://doi.org/10.3322/caac.21763.

[2] M. A. Lisio, L. Fu, A. Goyeneche, Z. H. Gao, and C. Telleria, "High-Grade Serous Ovarian Cancer: Basic Sciences, Clinical and Therapeutic Standpoints," *Int. J. Mol. Sci.*, vol. 20, no. 4, Feb. 2019, doi: 10.3390/IJMS20040952.

[3] M. Strobl *et al.*, “Adaptive therapy for ovarian cancer: An integrated approach to PARP inhibitor scheduling.,” *bioRxiv : the preprint server for biology*. United States, Mar. 2023. doi: 10.1101/2023.03.22.533721.

[4] G. Y. Q. Han *et al.*, “Ecological and evolutionary dynamics to design and improve ovarian cancer treatment.,” *Clin. Transl. Med.*, vol. 14, no. 9, p. e70012, Sep. 2024, doi: 10.1002/ctm2.70012.

[5] Ł. Biegała, A. Gajek, A. Marczak, and A. Rogalska, “PARP inhibitor resistance in ovarian cancer: Underlying mechanisms and therapeutic approaches targeting the ATR/CHK1 pathway,” *Biochim. Biophys. acta. Rev. cancer*, vol. 1876, no. 2, Dec. 2021, doi: 10.1016/J.BBCAN.2021.188633.

[6] R. T. Neff, L. Senter, and R. Salani, “BRCA mutation in ovarian cancer: testing, implications and treatment considerations,” *Ther. Adv. Med. Oncol.*, vol. 9, no. 8, p. 519, Aug. 2017, doi: 10.1177/1758834017714993.

[7] S. Banerjee *et al.*, “Maintenance olaparib for patients with newly diagnosed advanced ovarian cancer and a BRCA mutation (SOLO1/GOG 3004): 5-year follow-up of a randomised, double-blind, placebo-controlled, phase 3 trial,” *Lancet Oncol.*, vol. 22, no. 12, pp. 1721–1731, Dec. 2021, doi: 10.1016/S1470-2045(21)00531-3/ATTACHMENT/58691A46-326A-4D66-8A97-96131E589AAB/MMC1.PDF.

[8] H. Li, Z. Y. Liu, N. Wu, Y. C. Chen, Q. Cheng, and J. Wang, “PARP inhibitor resistance: the underlying mechanisms and clinical implications,” *Mol. Cancer*, vol. 19, no. 1, Jun. 2020, doi: 10.1186/S12943-020-01227-0.

[9] S. M. Noordermeer and H. van Attikum, “PARP Inhibitor Resistance: A Tug-of-War in BRCA-Mutated Cells,” *Trends Cell Biol.*, vol. 29, no. 10, pp. 820–834, Oct. 2019, doi: 10.1016/J.TCB.2019.07.008.

[10] E. K. Lee and U. A. Matulonis, “PARP Inhibitor Resistance Mechanisms and Implications for Post-Progression Combination Therapies,” *Cancers (Basel).*, vol. 12, no. 8, pp. 1–25, Aug. 2020, doi: 10.3390/CANCERS12082054.

[11] R. T. Davis *et al.*, “Transcriptional diversity and bioenergetic shift in human breast cancer metastasis revealed by single-cell RNA sequencing.,” *Nat. Cell Biol.*, vol. 22, no. 3, pp. 310–320, Mar. 2020, doi: 10.1038/s41556-020-0477-0.

[12] M. Milacic *et al.*, “The Reactome Pathway Knowledgebase 2024,” *Nucleic Acids Res.*, vol. 52, no. D1, pp. D672–D678, Jan. 2024, doi: 10.1093/nar/gkad1025.

[13] H. Cui, H. Maan, M. C. Vladoiu, J. Zhang, M. D. Taylor, and B. Wang, “DeepVelo: deep learning extends RNA velocity to multi-lineage systems with cell-specific kinetics,” *Genome Biol.*, vol. 25, no. 1, p. 27, 2024, doi: 10.1186/s13059-023-03148-9.

[14] V. Bergen, M. Lange, S. Peidli, F. A. Wolf, and F. J. Theis, “Generalizing RNA velocity to transient cell states through dynamical modeling,” *Nat. Biotechnol.*, vol. 38, no. 12, pp. 1408–1414, 2020, doi: 10.1038/s41587-020-0591-3.

[15] Z. Chen, W.C. King, A. Hwang, M. Gerstein, and J. Zhang, “DeepVelo: Single-cell transcriptomic deep velocity field learning with neural ordinary differential equations,” *Sci. Adv.*, 8, eabq3745 (2022). doi: 10.1126/sciadv.abq3745.

[16] M. A. R. Strobl *et al.*, “To modulate or to skip: De-escalating PARP inhibitor maintenance therapy in ovarian cancer using adaptive therapy,” *Cell Syst.*, vol. 15, no. 6, pp. 510-525.e6, Jun. 2024, doi: 10.1016/j.cels.2024.04.003.

[17] G. S. França *et al.*, “Drug-induced adaptation along a resistance continuum in cancer cells,” *bioRxiv*, p. 2022.06.21.496830, Jan. 2022, doi: 10.1101/2022.06.21.496830.

[18] Z. Xie *et al.*, “Gene Set Knowledge Discovery with Enrichr,” *Curr. Protoc.*, vol. 1, no. 3, p. e90, Mar. 2021, doi: https://doi.org/10.1002/cpz1.90.

[19] P. Jelinic and D. A. Levine, “New Insights into PARP Inhibitors’ Effect on Cell Cycle and Homology-Directed DNA Damage Repair,” *Mol. Cancer Ther.*, vol. 13, no. 6, pp. 1645–1654, Jun. 2014, doi: 10.1158/1535-7163.MCT-13-0906-T.

[20] N. Schultz, E. Lopez, N. Saleh-Gohari, and T. Helleday, “Poly(ADP-ribose) polymerase (PARP-1) has a controlling role in homologous recombination,” *Nucleic Acids Res.*, vol. 31, no. 17, pp. 4959–4964, Sep. 2003, doi: 10.1093/nar/gkg703.

[21] M. Kanehisa and S. Goto, “KEGG: kyoto encyclopedia of genes and genomes.,” *Nucleic Acids Res.*, vol. 28, no. 1, pp. 27–30, Jan. 2000, doi: 10.1093/nar/28.1.27.

[22] T. Li, C. Copeland, and A. Le, “Glutamine Metabolism in Cancer.,” *Adv. Exp. Med. Biol.*, vol. 1311, pp. 17–38, 2021, doi: 10.1007/978-3-030-65768-0_2.

[23] D. Adamoski *et al.*, “Molecular mechanism of glutaminase activation through filamentation and the role of filaments in mitophagy protection,” *Nat. Struct. Mol. Biol.*, vol. 30, no. 12, pp. 1902–1912, 2023, doi: 10.1038/s41594-023-01118-0.

[24] D. Slade, “PARP and PARG inhibitors in cancer treatment.,” *Genes Dev.*, vol. 34, no. 5–6, pp. 360–394, Mar. 2020, doi: 10.1101/gad.334516.119.

[25] M. Nakamura, T. Obata, T. Daikoku, and H. Fujiwara, “The Association and Significance of p53 in Gynecologic Cancers: The Potential of Targeted Therapy.,” *Int. J. Mol. Sci.*, 20, 5482, (2019). doi: 10.3390/ijms20215482.

[26] E. Crosas-Molist, R. Samain, L. Kohlhammer, J. L. Orgaz, S. L. George, O. Maiques, J. Barcelo, V. Sanz-Moreno., “Rho GTPase signaling in cancer progression and dissemination,” *Physiological Reviews*,102:1, pp. 455–510,

(2022) doi: 10.1152/physrev.00045.2020.

[27] H.C. Yoo, Y.C. Yu, Y. Sung, and J. M. Han, “Glutamine reliance in cell metabolism.,” *Exp. Mol. Med.*, **52**, 1496–1516 (2020). doi: 10.1038/s12276-020-00504-8.

[28] A. Bansal and M. C. Simon, “Glutathione metabolism in cancer progression and treatment resistance.,” *J. Cell Biol.*, vol. 217, no. 7, pp. 2291–2298, Jul. 2018, doi: 10.1083/jcb.201804161.

[29] Y. Hao, T. Stuart, M.H. Kowalski, S. Choudhary, *et al.*, “Dictionary learning for integrative, multimodal and scalable single-cell analysis,” *Nat. Biotechnol.*, vol. 42, no. 2, pp. 293–304, 2024, doi: 10.1038/s41587-023-01767-y.

[30] E. Becht *et al.*, “Dimensionality reduction for visualizing single-cell data using UMAP,” *Nat. Biotechnol.*, vol. 37, no. 1, pp. 38–44, 2019, doi: 10.1038/nbt.4314.

[31] G. La Manno *et al.*, “RNA velocity of single cells,” *Nature*, vol. 560, no. 7719, pp. 494–498, 2018, doi: 10.1038/s41586-018-0414-6.

[32] I. Virshup *et al.*, “The scverse project provides a computational ecosystem for single-cell omics data analysis,” *Nat. Biotechnol.*, vol. 41, no. 5, pp. 604–606, 2023, doi: 10.1038/s41587-023-01733-8.

[33] C. Rackauckas and Q. Nie, “DifferentialEquations.jl – A Performant and Feature-Rich Ecosystem for Solving Differential Equations in Julia,” *J. Open Res. Softw.*, vol. 5, p. 15, 2017, [Online]. Available: https://api.semanticscholar.org/CorpusID:64912314

[34] M. A. R. Strobl *et al.*, “Turnover Modulates the Need for a Cost of Resistance in Adaptive Therapy,” *Cancer Res.*, vol. 81, no. 4, pp. 1135–1147, Feb. 2021, doi: 10.1158/0008-5472.CAN-20-0806.

FIGURES

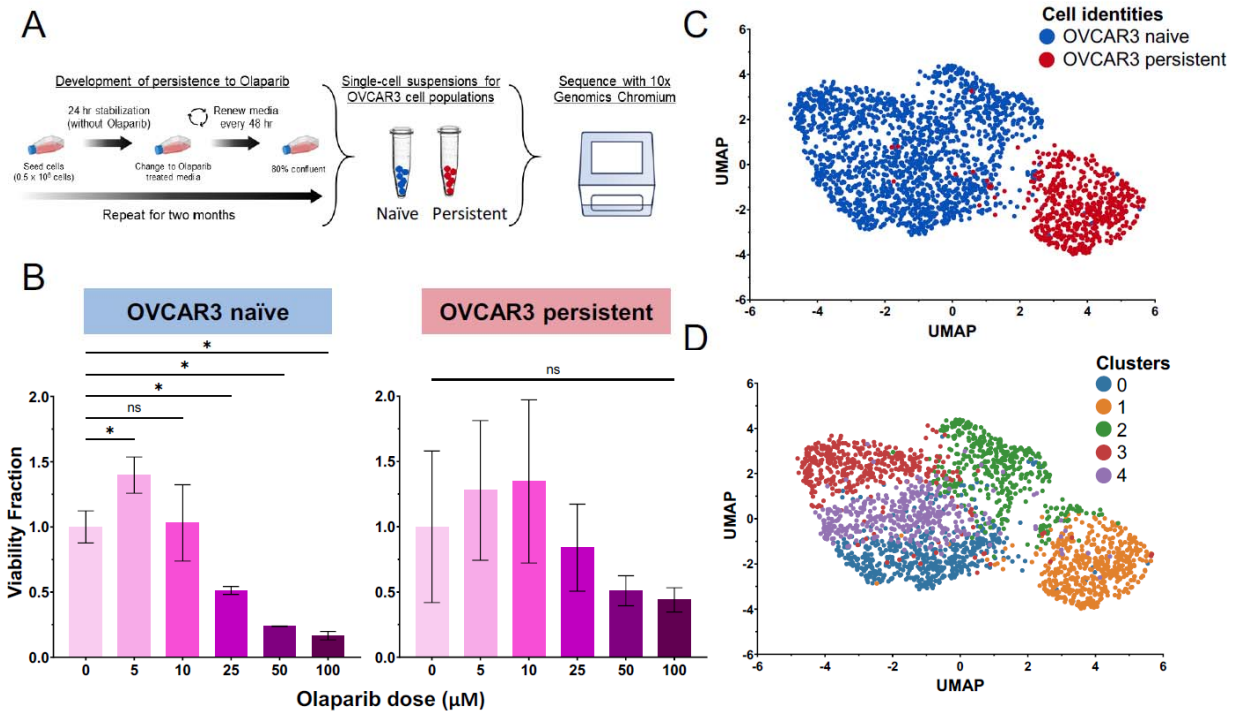

Figure 1. Divergent evolutionary trajectory captured by Olaparib persistence in OVCAR3 at single-cell resolution. **A,** Schematic of the cell culturing process and development of Olaparib persistence. OVCAR3 cells were cultured in 10μM Olaparib treated media for two months until persistence evolved. Single-cell suspensions were transcriptomically sequenced using the 10x Genomic Chromium platform. **B,** A one-week CCK-8 clonogenic assay shows cell viability fractions as low as 0.1659 for OVCAR3 naïve populations (n=3) at higher Olaparib doses (darker purple). The persistent population shows a 2-fold larger cell viability fraction of 0.4397 at high Olaparib doses compared to the parental cell lines (n=3). **C,** UMAP visualization of single cell RNA-sequencing data labeled by cell type (naïve cells, n=1712, blue and persistent cells, n=550, red). **D**, Graph-based clustering identified 5 distinct clusters from the single-cell data, where persistent cells dominated cluster 1.

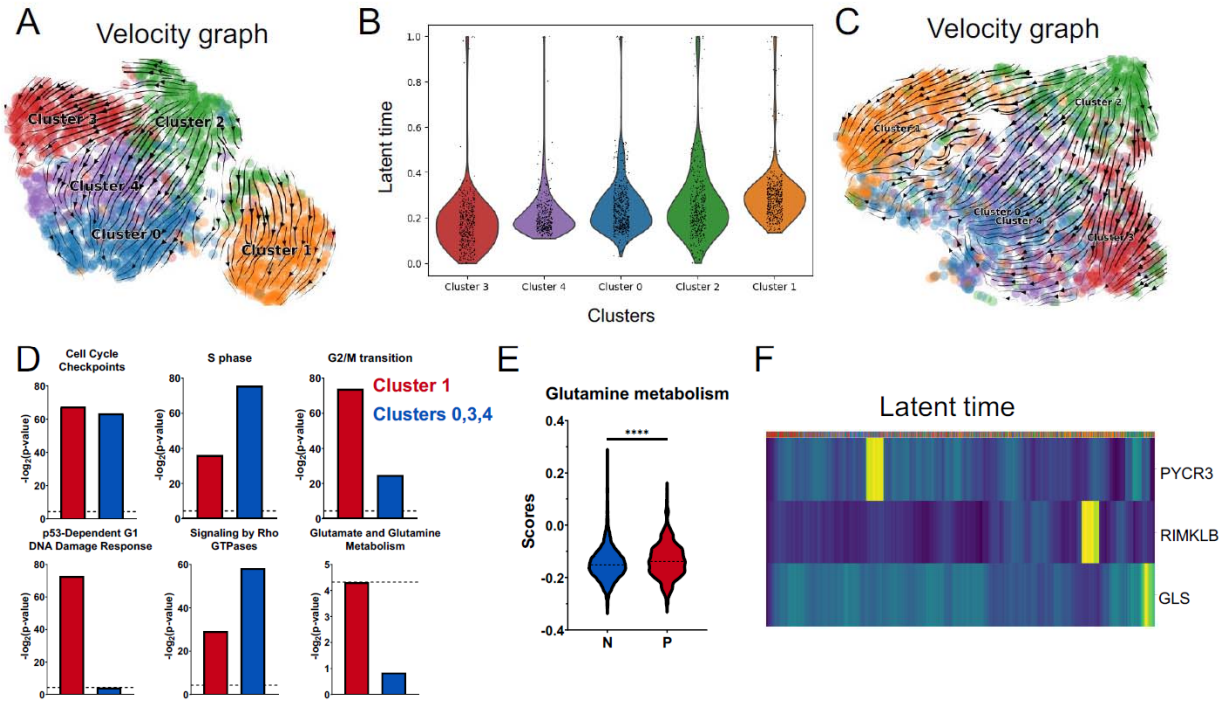

Figure 2. Transcriptomic differences between naïve and persistent populations indicate persistence dependence towards the glutamine metabolism. A, Velocity graph using the scVelo pipeline on the entire dataset (naïve and persistent populations combined) showed RNA velocities pointing towards cluster 1 which has a higher proportion of persistent cells. **B**, Clusters ordered based on the velocity-derived latent time obtained from the RNA velocity of each cell suggests that cells in cluster 3 (highest in naïve cell proportion) would be the starting point of persistence development moving towards a transcriptomic state similar to cells in cluster 1. **C**, Velocity graph using the DeepVelo algorithm by training a variational autoencoder predicted that the RNA velocity for the dataset were directed towards cluster 1. **D**, Differentially expressed genes for each cluster were obtained (min.pct=0.25, logfc.threshold=0.25). These were input into Enrichr to obtain the pathways primarily naïve (clusters 0, 3, 4) and persistent (cluster 1) clusters under the Reactome database. The p-values given for these Reactome pathways were determined using the Fisher's exact test. For both naïve and persistent clusters, cell cycle check points resulted in a top pathway ($p<0.05$). However, glutamate and glutamine metabolism were more highly expressed in the resistant cluster ($p<0.05$) compared to naïve clusters ($p>0.05$). **E**, After evaluating 42 unique metabolic pathways and calculating a pathway score for each cell in the dataset, the glutamine metabolism expressed significant difference between naïve and persistent populations ($p<0.0001$), using the Mann-Whitney test. **F**, Heatmap of the expression of the glutamine metabolism genes studied throughout the DeepVelo latent time. The GLS gene which catalyzes the conversion of glutamine into glutamate, is expressed at the end of the latent time.

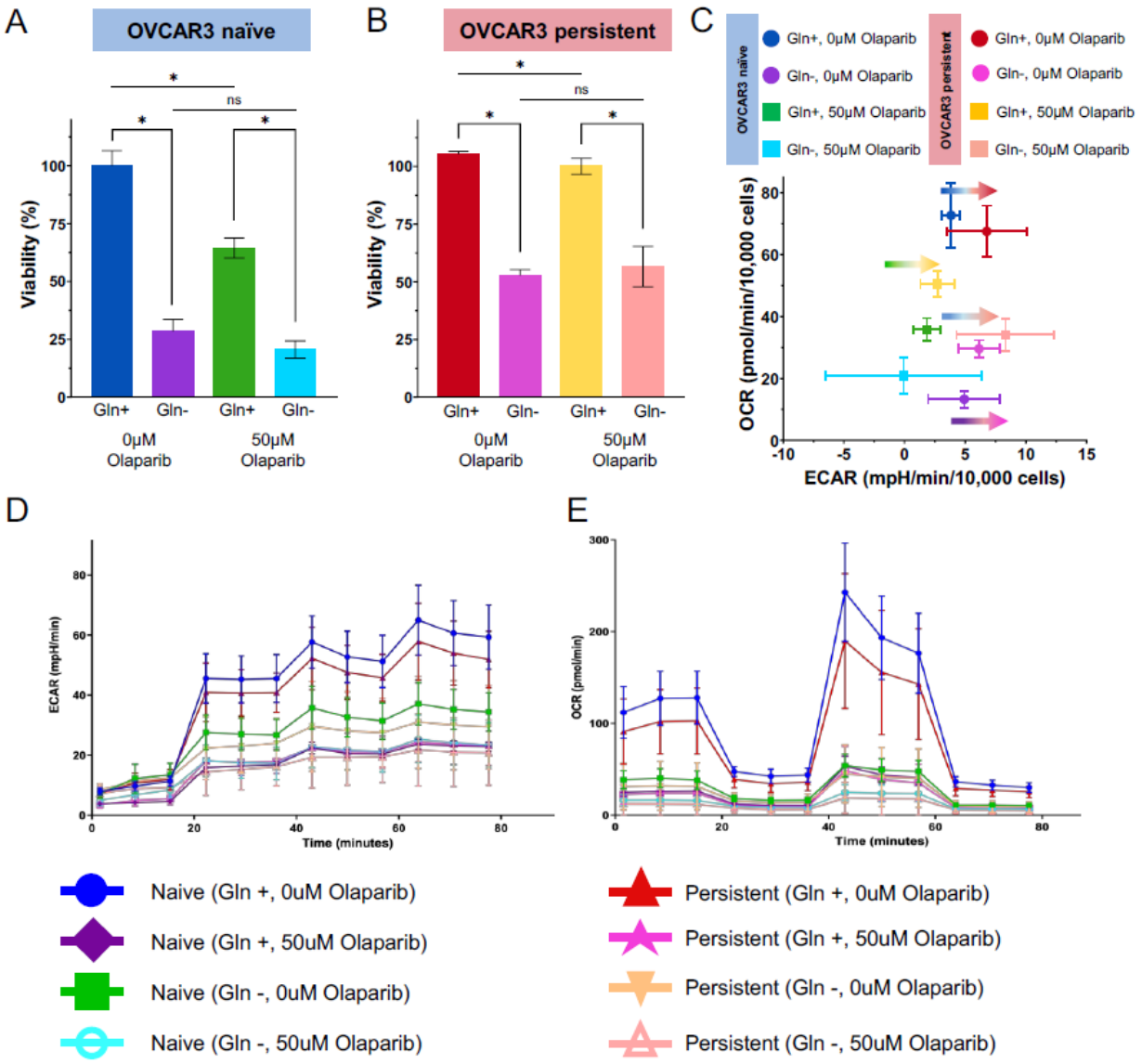

Figure 3. OVCAR3 persistent cells demonstrate high viability under Olaparib treated and glutamine deprived conditions. A, Viability assay of OVCA3 naïve cells treated with Olaparib in absence or presence of Gln. **B,** Viability assay of OVCA3 persistent cells treated with Olaparib in absence or presence of Gln. Viability is measured using CCK8 kit and data is the results of 3 biological replicates with 4 technical replicates in each biological replicates. Student t-test is used for analysis. **C,** OCR/ECAR analysis of the naïve and persistent OVCAR3 cells from Seahorse assay. Arrows show the transition toward more glycolysis under PARPi treatment. **D,** Extracellular acidification rate (ECAR) of OVCA3 cells in conditions similar to A. **E)** Oxygen consumption rate (OCR) of OVCA3 cells.

$$\frac{dN}{dt} = r_N\left(1 - \frac{N+P}{K_N}\right) - \alpha_N PARP * N - \beta_N(1 - GLN) * N \qquad \frac{dP}{dt} = r_P\left(1 - \frac{P+N}{K_P}\right) - \alpha_P PARP * P - \beta_P(1 - GLN) * P$$

$$T(t) = N(t) + P(t)$$

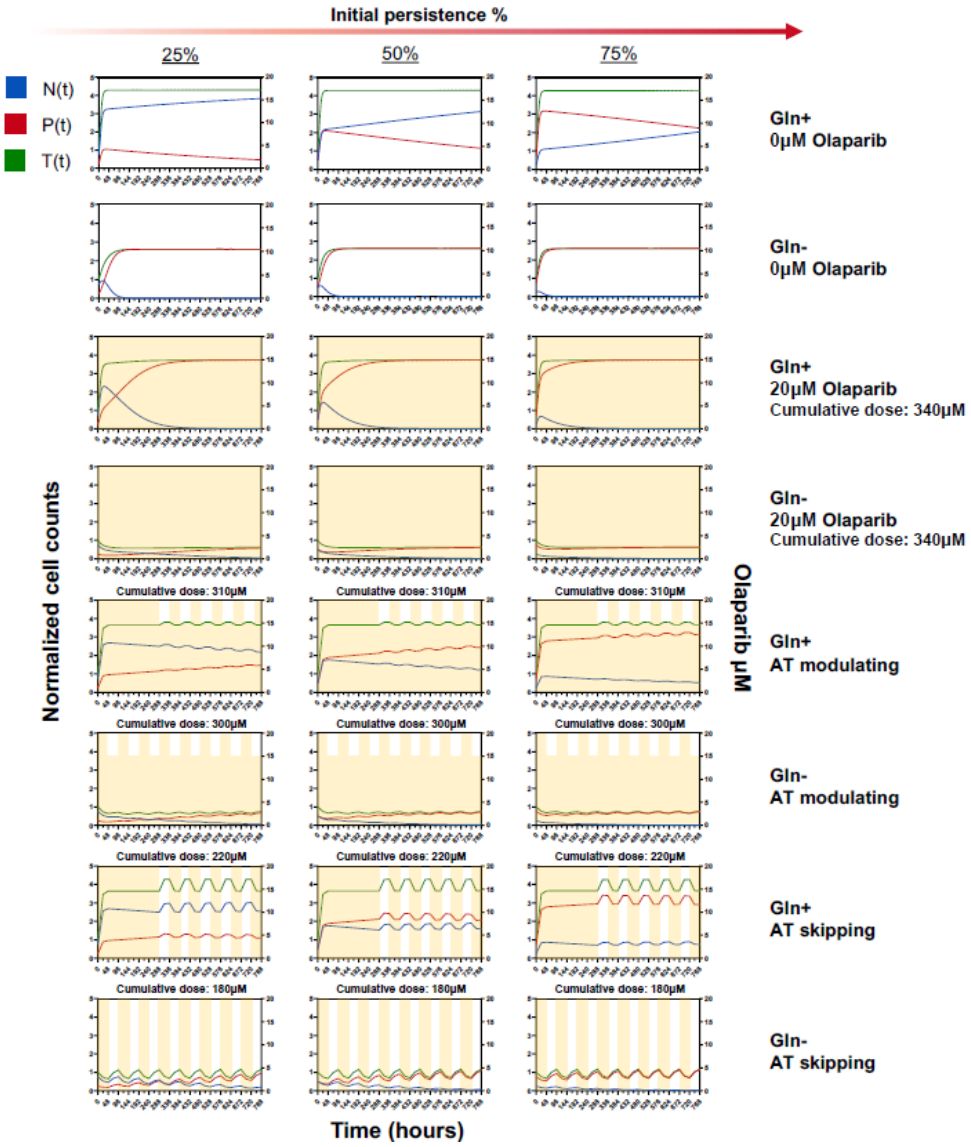

Figure 4. Mathematical models showed different growth dynamics of OVCAR3 naïve and persistent cells under different environmental conditions. OVCAR3 naïve and OVCAR3 persistent growth dynamics were estimated logistic growth curves computed on the normalized cell counts. Growth rates and carrying capacities for both OVCAR3 naïve and OVCAR3 persistent cells were parameterized in Julia using growth data under untreated and glutamine-added conditions (0μM Olaparib/Gln+). Using data from all other media conditions (0μM Olaparib/Gln-, 50μM Olaparib/Gln+, 50μM Olaparib/Gln-), an effect of treatment and glutamine deprivation linear terms were estimated. The resulting parameters were used to create co-culture simulations show the effects of different media conditions on the growth dynamics of sensitive (blue), resistant (red) and total (green) populations. The different initial persistence percentage shows that sensitive cells will dominate in the population only the initial persistence is

25% and the media is untreated, and glutamine is added. While treatment alone and glutamine deprivation alone each contribute to a decrease in the total population, this reduction is further amplified when glutamine deprivation and Olaparib are applied. Adaptive therapy simulation show that evolutionary treatment delivery reduces the cumulative drug dosage compared to continuous drug delivery. Different adaptive therapy schedules (AT modulating and AT skipping) were tested under glutamine added and deprived conditions. AT skipping under glutamine deprived conditions achieved the same treatment efficiency as the continues delivery of treatment with a much lower cumulative treatment dose.